Chemical Engineering Journal 392 (2020) 123640

Contents lists available at ScienceDirect

Chemical Engineering Journal

journal homepage: www.elsevier.com/locate/cej

Efficient removal of perfluorooctanoic acid by persulfate advanced oxidative degradation: inherent roles of iron-porphyrin and persistent free radicals

Wenze He[1], Yuan Zhu[1], Guangming Zeng*, Yi Zhang*, Yingrong Wang, Mingjuan Zhang, Huai Long, Wangwang Tang

College of Environmental Science and Engineering, Hunan University and Key Laboratory of Environmental Biology and Pollution Control (Hunan University), Ministry of Education, Changsha 410082, China

HIGHLIGHTS

- Inspired by biomimetic materials, a heterogeneous catalyst was constructed based on iron-porphyrin loaded biochar.
- The system degraded PFOA rapidly and effectively, and the degradation pathways and reaction mechanism were proposed.
- The system could maintain the efficient degradation under original strong acidic conditions without pH adjustment.

GRAPHICAL ABSTRACT

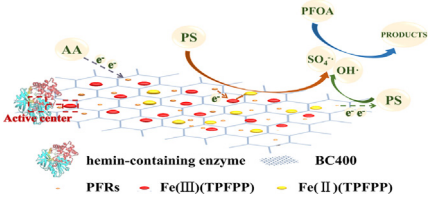

ARTICLE INFO

Keywords:
Perfluorinated compounds
Iron-porphyrin
Biochar
Persulfate
Advanced oxidation

ABSTRACT

Perfluorooctanoic acid (PFOA) is a persistent and bioaccumulative refractory organic pollutant, which has aroused great concern on its environmental fate. Herein, inspired by biomimetic materials, a preeminent heterogeneous catalyst, iron-porphyrin loaded biochar (Fe(TPFPP)/BC) was constructed to activate persulfate (PS) for PFOA degradation. Moreover, the existence of persistent free radicals (PFRs) on biochar could transfer electrons to iron-porphyrin and PS to directly or indirectly speed up the generation of $SO_4^{\cdot-}$ and OH·. By introducing ascorbic acid (AA) as an electronic circulation agent to maintain the concentration of PFRs, the Fe(TPFPP)/BC-PS-AA system could degrade 75.90% PFOA in 30 min, even reaching 90.88% with increasing reaction time. The effects of key factors on PFOA degradation were investigated. The reaction mechanism and degradation pathway were proposed as well. This work not only provides insights into the catalytic field by integrating biomimetic thought, but also provides an efficient method to degrade perfluorinated compounds (PFCs).

1. Introduction

Perfluorinated compounds (PFCs) are a class of anthropogenic chemicals, which contain a fully fluorinated hydrophobic alkyl chain and hydrophilic end group. They are widely used in industry and household surfactants and fire-fighting foams owing to their special properties, i.e. thermal stability and oxidative resistance [1]. Perfluorooctanoic acid, one of the most typical and common detected perfluorinated compounds, is usually detected in soil, surface water, and groundwater [2,3]. PFOA is bioaccumulative and possesses long-distance transmission capability. Once ingested into human body via food ingestion and drinking water, it can interfere with endocrine

* Corresponding authors.
E-mail addresses: zgming@hnu.edu.cn (G. Zeng), zyi@hnu.edu.cn (Y. Zhang).
[1] These authors contribute equally to this article.

https://doi.org/10.1016/j.cej.2019.123640
Received 29 August 2019; Received in revised form 25 November 2019; Accepted 28 November 2019
Available online 02 December 2019
1385-8947/

processes and induce potential reproductive and developmental toxicity [4–6].

It is difficult to naturally degrade PFOA due to its strong C-F bond (531.5 kJ·mol^{-1}) [7]. Many efforts have been made to dispose PFOA involving adsorption [8], sonolysis [9], advanced oxidation [10], etc [11,12]. Among them, adsorption is a flexible and effective strategy. However, it suffers from limitations such as eluent treatment [13–15]. Similarly, complicated operation and high energy consumption limit the large-scale application of sonolysis [16,17]. Alternatively, advanced oxidation process is a relatively ideal treatment method. It has the advantages of simplified operation and high versatility, high amenability and environmental compatibility [18,19]. In particular, it can efficiently convert organic pollutants into biodegradable small organic or inorganic substances within a short reaction time [20].

Persulfate based advanced oxidation process has been proved to be capable of degrade various refractory organic pollutants such as PFOA [21]. To activate persulfate, heat [22], radiation [23], electrolysis [24], and other methods [25–28] have been developed. Although heat activation and electrolysis activation can achieve satisfactory activation rate, they are energy-consuming and need complex equipment. Compared with these energy-based activation methods, heterogeneous catalysts have higher catalytic activity and reusability.

Biomimetic materials can cleverly exploit the structure of the organism which has been incessantly optimized and adjusted by the natural selection in the evolution [29–31]. They are quite attractive, especially the advantages of high efficiency and optimized structure [32,33]. Inspired by the concept, iron-porphyrin, a biomimetic model for the hemin-containing enzymes, awakened our interest to construct an efficient catalyst. Iron-porphyrin is a tetrapyrrole ring containing a divalent iron ion in the center, which is similar to the structure of the active site of peroxidase enzyme [34,35]. It could play an important role in transferring electrons during the catalytic process. Indeed, iron catalysts have been reported to possess excellent catalytic performance in activating persulfate [36,37], e.g., zero-valent iron [38] and ferroferric oxide [39]. Fe^0 has a favorable activation effect on persulfate, however, it suffers from poor stability. Free state Fe^{2+} suffers from being consumed rapidly due to its lower energy for persulfate activation. In relative terms, iron-porphyrin is more effective, stable, environmentally friendly, and can be used repeatedly. However, it might form catalytic inactive dimers in aqueous solution due to molecular aggregation, then resulting in the passivation of catalytic activity [40,41]. To overcome this drawback, immobilization is a feasible strategy to improve the stability and activity of iron-porphyrin [42,43], which could result in a significant increment in the reuse of iron-porphyrin [44].

Biochar is a carbonaceous material, which can be prepared from forestry and agricultural residues [45], sediment [46], domestic waste [47], etc [48,49]. It has abundant functional groups, high surface area and well developed pore structure [50]. According to the physical and chemical properties of biochar, it might be an ideal carrier to support iron-porphyrin and maintain the stability and activity of the biomimetic enzyme model. Especially, biochar contains rich persistent free radicals [51,52]. These PFRs are stable but reactive, and they can continuously provide electrons to other electron-acceptors, thus promote reactive oxygen species (ROS) formation in aqueous media [53,54]. Therefore, it is of great interest to investigate the situation when biochar and iron porphyrin meet.

Herein, inspired by biomimetic materials, a preeminent heterogeneous catalyst was constructed based on the hemin-containing enzyme active center mimic (iron-porphyrin), i.e. a camphor leaf biochar supported iron-porphyrin (Fe(TPFPP)/BC), which was employed as an activator of persulfate to generate radicals for oxidizing PFOA. Moreover, AA was introduced as an electronic circulation agent to regenerate the PFRs in biochar. The degradation efficiency, degradation process and reaction mechanism of PFOA by Fe(TPFPP)/BC-PS-AA system were elucidated. In addition, the effects of other influencing factors on the removal of PFOA were analyzed as well. This work not only provides a novel idea in catalytic field by integrating biomimetic thought, but also provides an efficient method to degrade PFCs.

2. Experimental sections

2.1. Chemicals and materials

Camphor leaves were obtained from Yuelu Mountain in Changsha, China. Perfluorooctanoic acid, iron-porphyrin (Fe(TPFPP)) and sodium persulfate were purchased from Aladdin. HPLC-grade ammonium acetate was produced by Anaqur Chemicals Supply corporation. HPLC-grade methanol was purchased from Merck. All other chemicals and solvents were analytical grade and supplied by Sinopharm Chemical Reagent limited corporation. Ultra-pure water was used throughout the PFOA degradation experiments.

2.2. Preparation of biochar

The collected camphor leaves were washed and over-dried at 110℃. The dried leaves were broken into granule and sieved through 100 mesh. Then they were pyrolysed at 400 ℃ for 6 h under N_2 flow condition. The obtained biochar (BC400) was rinsed with ultra-pure water and oven dried (110 ℃) for subsequent use.

2.3. Preparation of Fe(TPFPP)/BC

1 g BC400 and 0.1 g Fe(TPFPP) were dispersed into 50 mL DMF solution, and then mixed by magnetic stirring for 30 min. The mixture was transferred into a Teflon flask and placed inside a steel jar. The system was kept in a drying oven at 180 ℃ for 8 h. After cooling down to room temperature, the solid was washed several times and dried under vacuum at 40℃. The obtained sample was recorded as Fe (TPFPP)/BC.

2.4. Electron paramagnetic resonance (EPR) study

BC400 (0.02 g) was enclosed in a quartz capillary and then evaluated by EPR Spectrometer (EMX 10/12, Bruker, Germany). The resonance frequency was 9.76 GHz, the time constant was 40.96 ms, the microwave power was 19.92 mW, the modulation amplitude was 2.0 G, the modulation frequency was 100 kHz, the sweep time was 81.92 s, the sweep width was 200 G and the receiver gain was 1.0×10^3. The PFRs concentration of BC400 was quantified by EPR using a single crystal of ruby ($1.5 \times 1.5 \times 1.5$ mm^3) doped with 3.69×10^{15} Cr^{3+} mg^{-1} as a standard.

2.5. Characterization

The surface morphologies were analyzed by scanning electron microscopy (SEM) using a JSM-5600 LV microscope (JEO, Ltd., Japan). Fourier transform infrared (FTIR) spectra was recorded on NICOLET 5700 FTIR spectrometer. The crystal phase was obtained by X-ray diffraction (XRD) on D8 ADVANCE powder X-Ray diffractometer. The surface elemental composition and chemical state analyses were based on the results of X-ray photoelectron spectroscopy (XPS) (Thermo Fisher Scientific, UK).

2.6. Degradation experiments

50 mL PFOA solution was transferred into 150 mL conical flask. Then a certain amount of Fe(TPFPP)/BC were added the conical flask, followed by adding persulfate and AA to trigger the reaction. The PFOA degradation process was performed at 25 ± 1 ℃ by gas batch heating and mixed by a shaker (160 rpm). At this point, 10 mL aqueous sample was taken and quenched by 0.2 mL methanol. The mixture was filtered

through 0.22 μm membrane, followed by SPE cleanup.

The effects of key parameters (e.g. Fe(TPFPP)/BC dosage (0, 0.1, 0.2, 0.5, 1 and 2 g/L), persulfate concentration (0, 6.04, 12.06, 24.15, 36.23 and 60.39 mM), AA concentration (0, 1, 2, 5, 10 and 25 mM), initial pH (1, 2, 3, 5, 7, 9 and 11) and coexisting anions (Cl^- and CO_3^{2-}) (0, 0.01, 0.05, 0.1, 0.2 and 0.5 mM)) on the degradation of PFOA were investigated. And the radical quenching experiment was studied. The initial pH of the mixture was 2.89. The pH of the mixture was adjusted by 0.1 M HCl or NaOH solution. All experiments were carried out in triplicate.

The residual sulfate was treated by using ettringite precipitation method. The specific treatment steps were supplied in the support information.

2.7. Products analysis

PFOA and its decomposition products were analyzed by a high-performance liquid chromatograph (HPLC) Agilent 1290/6460 Triple Quad equipped with a mass spectrometer operated in negative ion electrospray ionization mode, and the quantification limits of PFOA was 9 ng/L (RSD less than 5.5%, S/N = 7.2, n = 6). PFOA and its decomposition products were separated by C_{18} column (2.1 × 100 mm; 1.8 μm, Agilent). The column was held at 30°C and the flow rate was 0.3 mL/min. The mobile phase consisted of (A) 10 mM ammonium acetate and (B) methanol. The eluent gradient was set to13 min. It was started with 40% B and maintained 1 min. Then B was increased to 100% in 6 min, then it was held for another 3.5 min. And finally B was returned to 40% over additional 2.5 min.

3. Results and discussion

3.1. EPR analysis

EPR spectroscopy was conducted to investigate the effect of PFRs in BC400, involving their concentration and species. A broad singlet EPR signal was observed of BC400 in Fig. 1. The g-factor and ΔH_{p-p} of BC400 was 2.0036 and 6.8000G, respectively. Since the g-factor of carbon-centered radicals with an adjacent oxygen atom was in the range of 2.0030–2.0040, while the g-factor of carbon-centered radicals was less than 2.0030 and that of oxygen centered radicals were larger than 2.0040 [55]. It means that carbon-centered radicals with an adjacent oxygen atom were dominant in BC400. In addition, the concentration of PFRs in BC400 reached 2.69 × 10^{19} spins/g.

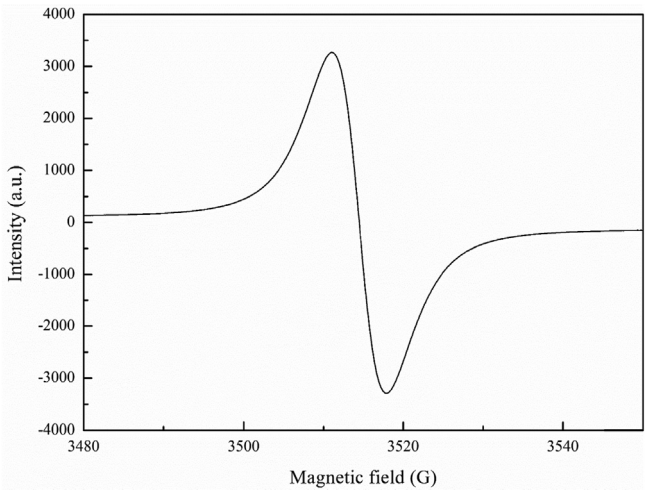

Fig. 1. EPR spectra of BC400.

3.2. Characterization

The morphology of BC400 and Fe(TPFPP)/BC was investigated by SEM. As seen in Fig. 2a, the pore size distribution was uniform and ordered closely on BC400. Obviously, a large specific surface area and a high adsorption site could be provided. When obtaining the Fe(TPFPP)/BC based adhesion effect, the iron-porphyrin spherical particles were highly uniform and dense on the biochar support (Fig. 2b). These results indicated that BC400 is an excellent support to disperse and stabilize iron-porphyrin. It was beneficial to immobilizing the artificial enzyme active center mimic and achieving an excellent catalytic effect.

Moreover, the composition of elements in BC400, iron-porphyrin and Fe(TPFPP)/BC were tested by XPS. A new band of iron was detected in the spectrum of Fe(TPFPP)/BC. Besides, the bands of nitrogen, carbon and oxygen had a marked increase compared to that of BC400 (Fig. 3a). As shown in C 1 s spectrum(Fig. 3b), the C = O binding energy of Fe(TPFPP)/BC is 287.3 eV, which both shifted 2.1 eV compared with BC400 and iron-porphyrin, and the percentage of C = O increased by 6.07% and 4.62%, respectively. These results indicated that the immobilization of iron-porphyrin on biochar would affect the chemical state of C. According to Fe 2p spectrum (Fig. 3c), Fe(TPFPP)/BC presented two new peaks at 711.24 eV and 724.42 eV compared to BC400, which were attributed to the existence of Fe species in Fe-N. While, there were almost no change in the chemical state of O and N (Fig. 3d and e). The above results suggested that Fe(TPFPP)/BC was successfully synthesized, and the structure of iron-porphyrin had no change in the preparation process, i.e. the biomimetic enzyme model on the Fe (TPFPP)/BC could give full play to its catalytic activity. Specific data for the binding energy of each electron and its proportion in BC400, iron-porphyrin and Fe(TPFPP)/BC was summarized in Table 1.

The crystal structure of materials was observed by XRD. The powder X-ray diffraction patterns of BC400, iron-porphyrin and Fe(TPFPP)/BC were shown in Fig. 4a. Fe(TPFPP)/BC displayed the basal diffraction peaks in the similar location with BC400, indicating that the iron-porphyrin immobilization took place on the surface and at the edges of biochar, which did not change the structure of biochar. The high purity of the sample during the immobilization process was also confirmed since no other crystalline impurity was detected.

To further verify the functional group structure of the obtained materials, BC400 and Fe(TPFPP)/BC were tested by FTIR (Fig. 4b). Because of the low iron-porphyrin loading amount on the support, the FTIR spectra of Fe(TPFPP)/BC was mainly based on the characteristic vibration bands of the groups of BC400. The bands at 1602 cm^{-1} and 1311 cm^{-1} in the spectrum of Fe(TPFPP)/BC were attributed to amine groups. The peak that appeared at 1749 cm^{-1} in the spectrum of BC400, which was attributed to C = O bonds, shifted to 1752 cm^{-1} in the spectrum of Fe(TPFPP)/BC. Meanwhile, a new absorption peak was observed at 700 cm^{-1}. These results indicated that the artificial enzyme active center mimic was anchored onto BC400 through covalent bonds, i.e. O = C-Cl.

3.3. Degradation process

Compared to PS alone system and Fe(TPFPP)/BC alone system, the Fe(TPFPP)/BC-PS-AA system could degrade PFOA efficiently and rapidly (Fig. 5a, b). 56.85% PFOA was degraded in just 5 min. After reacting for 30 min, the degradation efficiency was 75.90%, and then reached 90.88% in 12 h. To reveal the effect of different factors in the PFOA degradation process, a series of reaction parameters, e.g., Fe (TPFPP)/BC dosage, PS dosage, AA dosage, pH and coexisting anions were involved.

3.3.1. Impact of Fe(TPFPP)/BC dosage

Effects of different Fe(TPFPP)/BC dosages (0, 0.1, 0.2, 0.5, 1, 2 g/L) on the degradation of PFOA were investigated (Fig. 5c). The persulfate alone system only degraded 21.20% PFOA. In contrast, a steep rise of

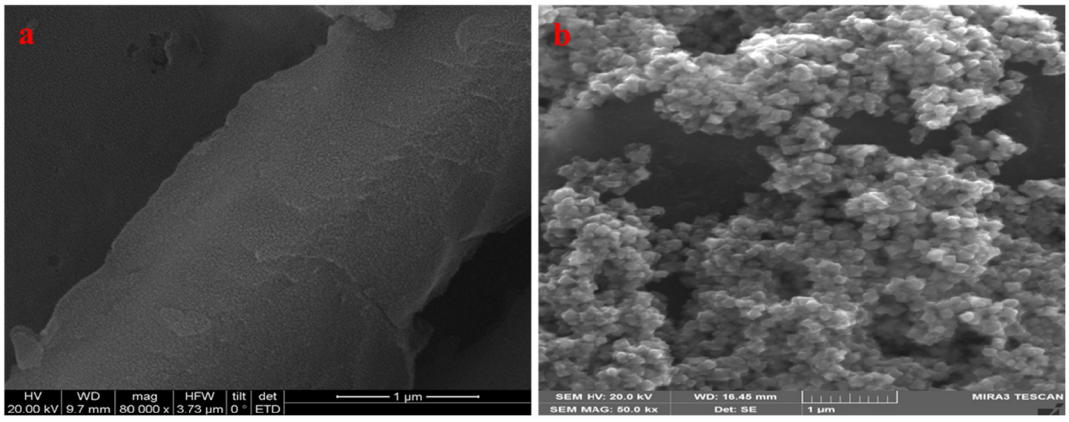

Fig. 2. SEM image of BC400 (a) and Fe(TPFPP)/BC (b).

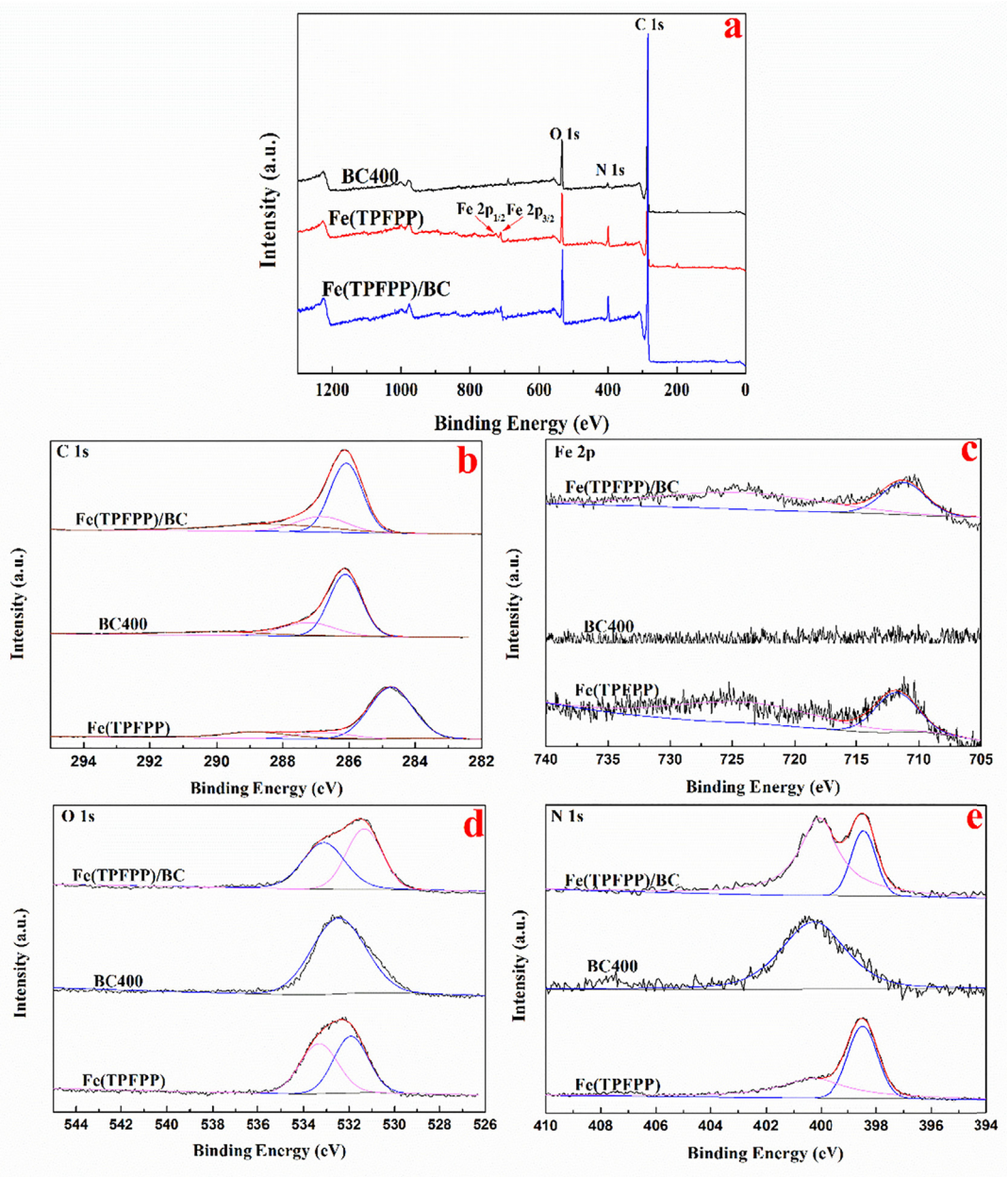

Fig. 3. XPS survey spectra (a), C 1s spectra (b), Fe 2p spectra (c), O 1s spectra (d) and N 1s spectra (e) of BC400, iron-porphyrin and Fe(TPFPP)/BC.

Table 1
Assignments of main spectral bands based on their binding energy (BE) for the core electrons of BC400, iron-porphyrin and Fe(TPFPP)/BC.

XPS spectra	Existential form of elements	BC400		Fe(TPFPP)		Fe(TPFPP)/BC	
		BE/eV	Percent of valence statea/%	BE/eV	Percent of valence statea/%	BE/eV	Percent of valence statea/%
C 1s	C–C	284.8	60.53	284.7	72.30	284.7	58.06
	C—OH	——	——	286.8	10.78	285.6	20.40
	C=O	289.2	15.47	288.8	16.92	287.3	21.54
O 1s	C=O	533.1	100	531.9	50.79	531.3	49.52
	C—OH	——	——	533.3	49.21	533.1	50.48
N 1s	Fe—N	——	——	398.5	50.99	398.4	24.81
	C—N	400.3	100	400.3	49.00	400.1	75.19
Fe	Fe—N	——	——	711.75	34.93	711.24	33.98
		——	——	724.23	65.07	724.42	66.02

degradation efficiency of PFOA was achieved when added Fe(TPFPP)/BC. With the Fe(TPFPP)/BC dosages increasing from 0.1 g/L to 1 g/L, the degradation efficiency of PFOA improved from 36.96% to 87.33%. The increase in degradation might attribute to the following aspects. Firstly, the amount of active sites and catalytic reaction centers increased with the increment of Fe(TPFPP)/BC dosage, which was in favor of persulfate activation and radicals generation for oxidizing PFOA. Next, it was noteworthy that the total PFRs on the biochar was positively related with the dosage of Fe(TPFPP)/BC. On the one hand, the growing PFRs could persistently provide electrons to iron-porphyrin, thereby speeding up activating persulfate. On the other hand, they could directly transfer electrons to persulfate to produce radicals. Nevertheless, the degradation efficiency of PFOA was not significantly improved when Fe(TPFPP)/BC varied from 1 g/L to 2 g/L. It was inferred that the active sites and catalytic reaction centers of activated persulfate had reached saturation and the contribution of adsorption was negligible.

3.3.2. Impact of persulfate concentration

Effects of various persulfate concentrations (0, 6.04, 12.08, 24.15, 36.23, 60.39 mM) were investigated as well. It was speculated that the PFOA degradation was dependent on the persulfate concentration. The degradation efficiency in Fe(TPFPP)/BC alone system was 36.35% (Fig. 5d). Because iron-porphyrin as hemin-containing enzymes active center mimic, it could function as an oxygen transfer reagent. The carried oxygen molecules could combine with electrons on BC400 to form O_2^{-}·[56]. And PFRs on BC400 could induce OH· generation in the presence of O_2 [51]. Once the system supplemented with persulfate, the existing Fe(TPFPP)/BC would activate persulfate to generate SO_4^{-}·, which could also trig other radicals generation (Eq. (1)–(5)) to degrade PFOA. When the persulfate concentration was increased to 60.39 mM, the degradation efficiency of PFOA reached 97.89%. It was important to note that overdose of persulfate could accelerate radical-scavenging, because excessive SO_4^{-}· could react with $S_2O_8^{2-}$ (Eq. (6) and (7)) and evoke self-consumption (Eqs. (8) and (9)). Obviously, an appropriate persulfate dosage would maintain high degradation efficiency of PFOA, meanwhile avoid materials waste.

$$SO_4^{-}\cdot + H_2O \rightarrow SO_4^{2-} + H^+ + OH\cdot \quad (1)$$

$$SO_4^{-}\cdot + H_2O \rightarrow HSO_4^{-} + OH\cdot \quad (2)$$

$$OH\cdot + OH\cdot \rightarrow H_2O_2 \quad (3)$$

$$OH\cdot + H_2O_2 \rightarrow H_2O + H_2\cdot \quad (4)$$

$$OH^- + H_2O_2 \leftrightarrow H_2O + HO_2^- \quad (5)$$

$$SO_4^{-}\cdot + S_2O_8^{2-} \rightarrow SO_4^{2-} + S_2O_8^{-}\cdot \quad (6)$$

$$SO_4^{-}\cdot + S_2O_8^{2-} \rightarrow 3SO_4^{2-} \quad (7)$$

$$SO_4^{-}\cdot + SO_4^{-}\cdot \rightarrow S_2O_8^{2-} \quad (8)$$

$$SO_4^{-}\cdot + SO_4^{-}\cdot \rightarrow 2SO_4^{2-} \quad (9)$$

3.3.3. Impact of AA concentration

As an electronic circulation agent, AA in the Fe(TPFPP)/BC-PS-AA system could “charge” to BC400, further influence the degradation of PFOA. The effects of different AA concentration (0, 1, 2, 5, 10, 20 mM) on the PFOA degradation were showed in Fig. 6a. AA could markedly promote the degradation efficiency of PFOA. With the addition of 1 mM AA, the degradation efficiency of PFOA increased by 11.68%, compared to AA free system. Certainly, AA could continuously supply electrons to

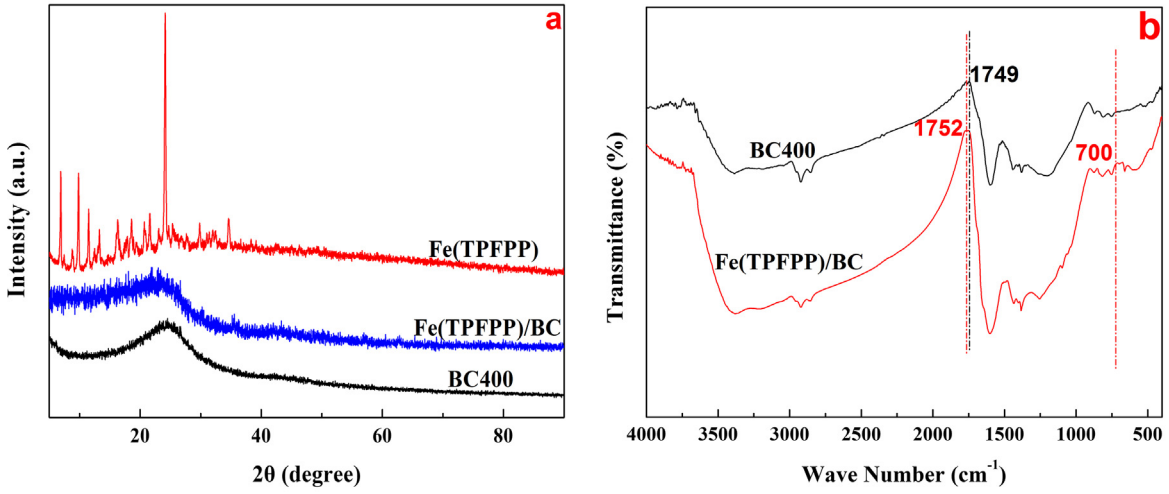

Fig. 4. (a) Powder X-ray diffraction patterns of BC400, Fe(TPFPP) and Fe(TPFPP)/BC; (b) FTIR spectra of BC400 and Fe(TPFPP)/BC.

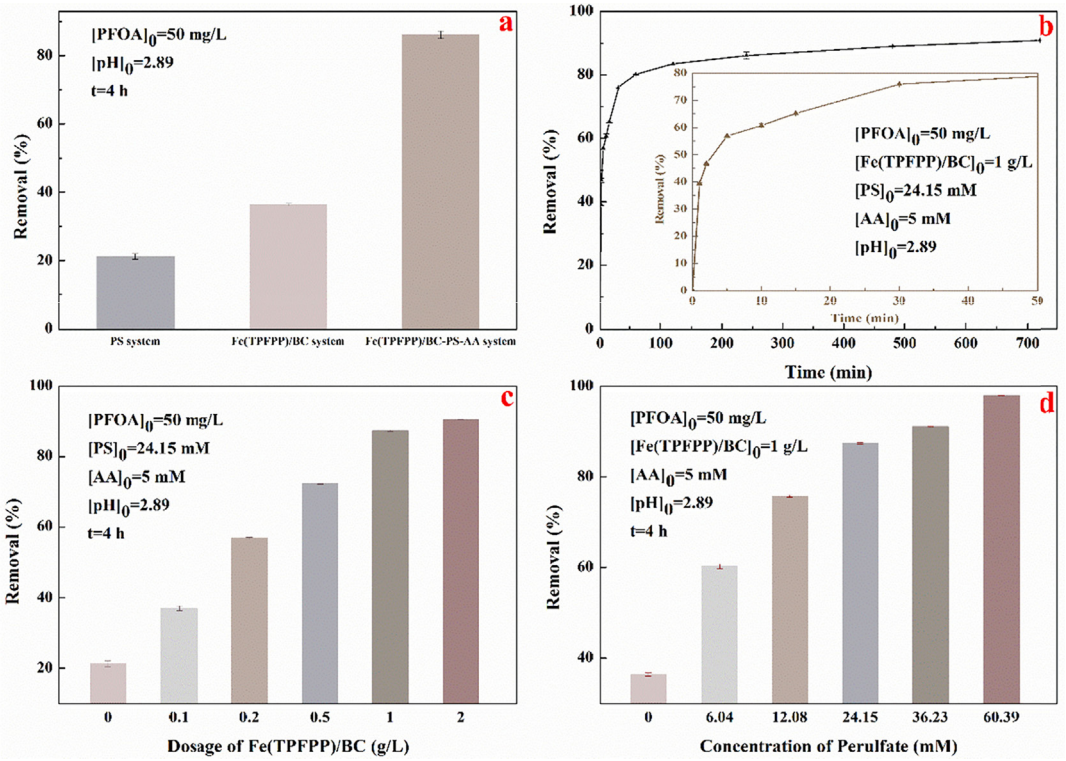

Fig. 5. Influence of system (a), time (b), Fe(TPFPP)/BC dosage (c) and persulfate concentration (d) on PFOA degradation.

BC400 and regenerated the consumed PFRs, thereby maintaining the sustainable electron transfer process from BC400 to porphyin and persulfate. It made system exhibit a higher efficiency in the generation of radicals, thereby enhancing PFOA degradation process.

3.3.4. *Impact of initial pH*

The initial solution pH was another critical operation parameter that might influence the Fe(TPFPP)/BC-PS-AA system, involving the oxidant activity, the radical oxidation potential, the ionization degree of organics, and the surface charge of solid, etc [57]. Various initial pH

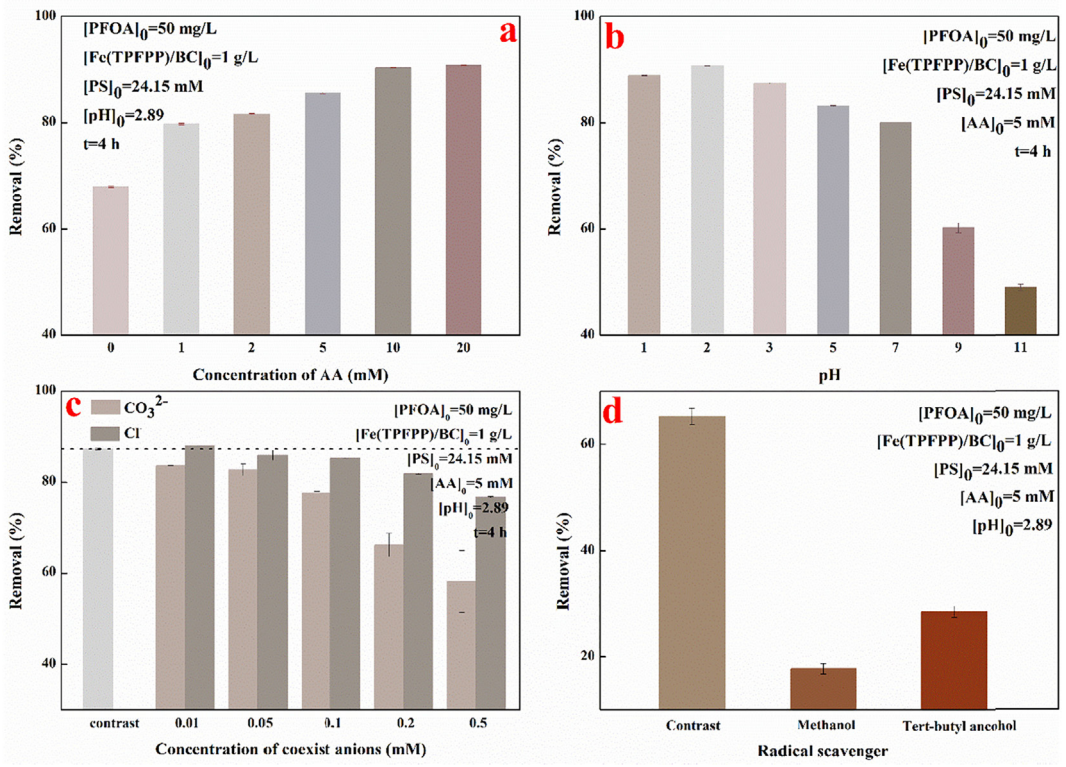

Fig. 6. Influence of AA concentration (a), initial pH (b), coexist anions (c) and radical scavengers (d) on PFOA degradation.

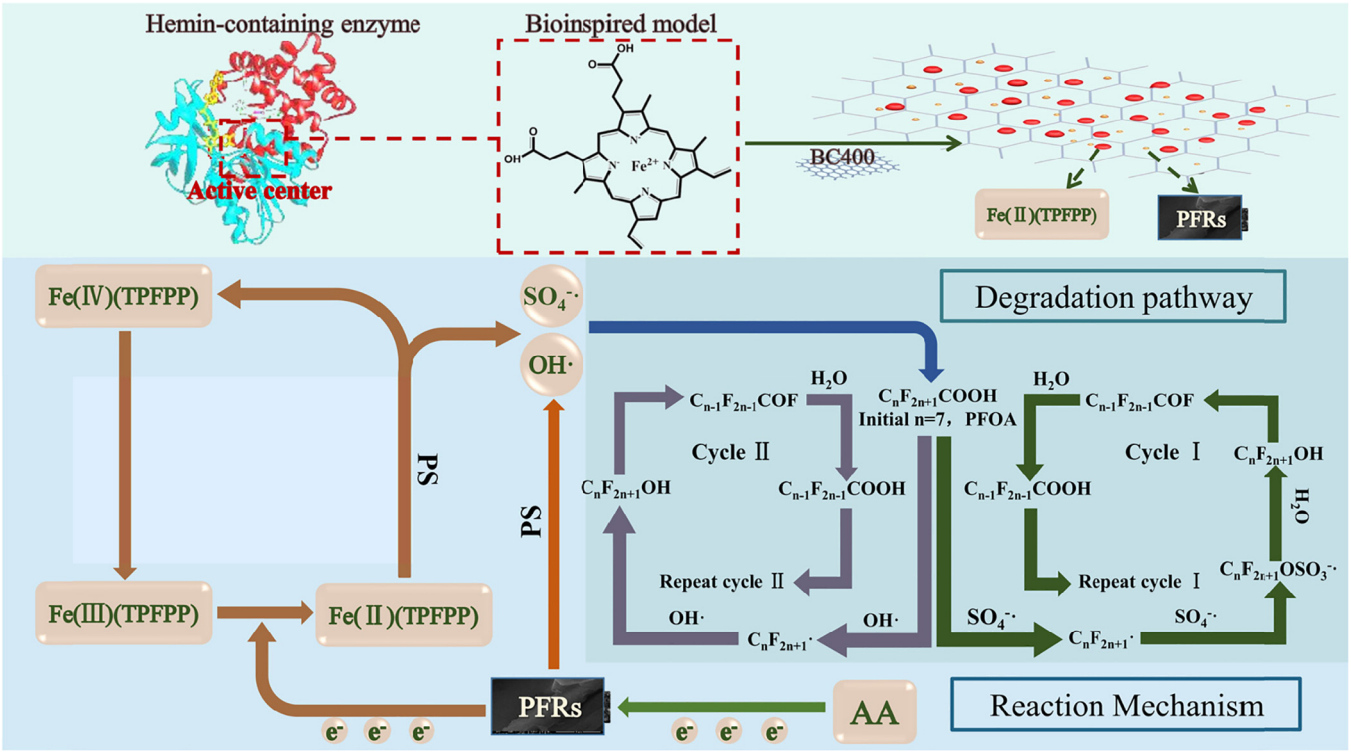

Fig. 7. Proposed mechanism in PFOA degradation process by Fe(TPFPP)/BC-PS-AA system.

conditions (1, 2, 3, 5, 7, 9, 11) were investigated for the degradation of PFOA by Fe(TPFPP)/BC-PS-AA system. The degradation efficiency of PFOA under acidic condition was generally superior to that under alkaline condition (Fig. 6b). The maximum degradation efficiency was 90.69% with pH = 2, by contrast, the efficiency was only 49.02% when pH was 11. The possible reasons were summarized as follows: 1) $SO_4^{\cdot-}$ could be formed by H^+ catalysis under acidic condition as shown in Eq. (10) and (11). 2) Quite a number of $SO_4^{\cdot-}$ and OH· were depleted under alkaline condition. Under alkaline conditions, $SO_4^{\cdot-}$ would convert into OH· (Eq. (2) and (12)). Then, OH· could react with itself and generated H_2O_2 (Eq. (3)). Then, the generated H_2O_2 could react with $SO_4^{\cdot-}$ (Eq. (13)), which would increase the depletion of $SO_4^{\cdot-}$. 3) When the pH was around 7, some of the formed $SO_4^{\cdot-}$ would convert into OH· (Eq. (1)), and then OH· became the dominant radical in the system. OH· had a relatively poor reactivity compared to $SO_4^{\cdot-}$. 4) In addition, AA was easy to be oxidized in alkaline solution and lost the role of elector donor.

Notably, the pH of the unadjusted sample was 2.89, just located in the pH range of 1 to 3, where had excellent degradation efficiency. It means that the original sample without pH adjustment is suitable for direct processing with high degradation efficiency of PFOA in the proposed system. Fe(TPFPP)/BC could remain high catalytic activity in extreme environments by introducing enzyme active center mimic instead of using enzyme directly.

$$S_2O_8^{2-} + H^+ \rightarrow HS_2O_8^- \quad (10)$$

$$HS_2O_8^- \rightarrow SO_4^{\cdot-} + SO_4^{2-} + H^+ \quad (11)$$

$$SO_4^{\cdot-} + OH^- \rightarrow SO_4^{2-} + OH \quad (12)$$

$$S_2O_8^{2-} + H_2O_2 \leftrightarrow 2H^+ + 2SO_4^{2-} + O_2 \quad (13)$$

3.3.5. Impact of coexisting anions

The coexisting anions in solution would also influence the degradation of PFOA. To test the effect of coexisting anions, two commonly coexisting anions, i.e. Cl^- and CO_3^{2-}, were explored. As shown in Fig. 6c, CO_3^{2-} showed a stronger inhibitory effect on the degradation of PFOA than Cl^-. When the concentration of CO_3^{2-} increased to 0.5 Mm,the degradation efficiency was reduced by 27.48% compared to the control group. Both Cl^- and CO_3^{2-} could react with $SO_4^{\cdot-}$ and generated other radicals (Eq. (14)–(16)), and the redox potential was $SO_4^{\cdot-} > Cl\cdot > Cl_2^{\cdot-} > CO_3^{\cdot-}$[58]. Moreover, the original pH was 2.89, just located in the optimum pH range (1–3). In this pH range, the Fe(TPFPP)/BC-PS-AA system had excellent PFOA degradation efficiency. But the addition of CO_3^{2-} would increase pH of system (Eq. (17)). These explained why CO_3^{2-} showed great inhibitory effect on the degradation of PFOA, and why PFOA degradation was enhanced slightly when the concentration of Cl^- was maintained at a low level.

$$SO_4^{\cdot-} + Cl^- \rightarrow SO_4^{2-} + Cl\cdot \quad (14)$$

$$Cl\cdot + Cl^- \rightarrow Cl_2^{\cdot-} \quad (15)$$

$$SO_4^{\cdot-} + CO_3^{2-} \rightarrow SO_4^{2-} + CO_3^{\cdot-} \quad (16)$$

$$CO_3^{2-} + H^+ \rightarrow HCO_3^- \quad (17)$$

3.3.6. Radical quenching experiment

To verify the main species of radicals worked in PFOA degradation, methanol was adopted as the scavenger for $SO_4^{\cdot-}$ and OH·, and *tert*-butyl alcohol for OH·. These scavengers show different reaction rate constant with $SO_4^{\cdot-}$ and OH·. The reaction rate constants of methanol with $SO_4^{\cdot-}$ and OH· are $3.2 \times 10^6\ M^{-1}\cdot s^{-1}$ and $9.7 \times 10^8\ M^{-1}\cdot s^{-1}$, respectively. By contrast, the reaction rate constants of *tert*-butyl alcohol with $SO_4^{\cdot-}$ and OH· are $4 \sim 9.1 \times 10^5\ M^{-1}\cdot s^{-1}$ and $3.8 \sim 7.6 \times 10^8\ M^{-1}\cdot s^{-1}$ [59]. As shown in Fig. 6d, 65.27% PFOA could be degraded with no scavenger added into system. After adding scavenger, the degradation efficiency decreased to 17.72% (methanol) and 28.50% (*tert*-butyl alcohol), respectively. These results demonstrated that $SO_4^{\cdot-}$ was the dominant radical species worked in degradation process.

3.4. Reaction mechanism

Based on the results and analysis above, Fe(TPFPP)/BC-PS-AA

system could degrade PFOA quickly and efficiently. During the PFOA degradation process, two kinds of radicals i.e. $SO_4^{\cdot-}$ and OH· were presumed to degrade PFOA. Accordingly, there were two different chemical reaction pathways to degrade PFOA by the Fe(TPFPP)/BC-PS-AA system, and the possible degradation pathways and intermediates were concluded in Fig. 7. In fact, this speculation matched the detection results of intermediates by LC-MS-MS in PFOA degradation process (Fig. S1).

Particularly, Fe(TPFPP)/BC displayed extremely strong catalytic activity on persulfate. In the activation process, Fe(II)(TPFPP) transformed into Fe(IV)(TPFPP) and the generated radicals reacted with PFOA, then Fe(IV)(TPFPP) turned into Fe(III)(TPFPP). PFRs on the biochar played an irreplaceable role in the electronic transfer process. On the one hand, it could supply electrons to iron-porphyrin, thereby speeding up the conversion of Fe(III)(TPFPP) to Fe(II)(TPFPP). On the other hand, PFRs could transfer electrons to persulfate directly, and then forming radicals. Certainly, Fe(TPFPP)/BC is an excellent catalyst, which is capable to give full play to the catalytic activity of iron-porphyrin similar to hemin-containing enzyme active center, while the PFRs from biochar are utilized completely as well.

During the whole reaction, AA acted as an electronic circulation agent, which constantly transferred electrons to biochar to regenerate the consumed PFRs, thereby maintained electron transfer process from biochar to iron-porphyrin.

4. Conclusion

In summary, inspired by biomimetic materials, a preeminent heterogeneous catalyst Fe(TPFPP)/BC was constructed to activate persulfate for PFOA degradation with AA as electronic circulation agent. The Fe(TPFPP)/BC-PS-AA system could degrade 75.90% PFOA in 30 min, and then reached 90.88% with increasing reaction time. The excellent degradation capability was attributed to the high catalytic activity of iron-porphyrin similar to the hemin-containing enzyme active center mimic, and the cooperative action of PFRs on biochar. In addition, PFRs could constantly supply electrons to iron-porphyrin and persulfate for accelerating the generation of $SO_4^{\cdot-}$ and OH· with the aid of AA. Especially, this system could maintain the efficient degradation under original strong acidic conditions without pH adjustment. This study shows that it is efficient and feasible to construct catalyst by introducing biomimetic thought, and biomimetic catalyst is expected and promising for degrading refractory organic pollutants.

Declaration of Competing Interest

The authors declare that they have no known competing financial interests or personal relationships that could have appeared to influence the work reported in this paper.

Acknowledgments

This study was financially supported by the National Natural Science Foundation of China (51521006, 51979102, 51508175, 51709285), the Program for Changjiang Scholars and Innovative Research Team in University (IRT-13R17), Science and Technology Plan Project of Hunan Province, China (2015SK2001), Natural Science Foundation of Hunan Province, China (2018JJ2046), China Postdoctoral Science Foundation (2016M600490, 2017T100462) and The Three Gorges Follow-up Research Project (2017HXXY-05).

Appendix A. Supplementary data

Supplementary data to this article can be found online at https://doi.org/10.1016/j.cej.2019.123640.

References

[1] D.L. Pan, S.N. Xiao, X.F. Chen, R.P. Li, Y.N. Cao, D.Q. Zhang, S.S. Pu, Z.C. Li, G.S. Li, H.X. Li, Efficient Photocatalytic Fuel Cell via Simultaneous Visible-Photoelectrocatalytic Degradation and Electricity Generation on a Porous Coral-like WO3/W Photoelectrode, Environ. Sci. Techno. 53 (2019) 3697–3706.
[2] Z. Sun, C. Zhang, H. Yan, C. Han, L. Chen, X. Meng, Q. Zhou, Spatiotemporal distribution and potential sources of perfluoroalkyl acids in Huangpu River Shanghai, China, Chemosphere 174 (2017) 127.
[3] S. Chen, X.C. Jiao, N. Gai, X.J. Li, X.C. Wang, G.H. Lu, H.T. Piao, Z. Rao, Y.L. Yang, Perfluorinated compounds in soil, surface water, and groundwater from rural areas in eastern China, Environ. Pollut. 211 (2016) 124–131.
[4] S. Chu, R.J. Letcher, D.J. Mcgoldrick, S.M. Backus, A New Fluorinated Surfactant Contaminant in Biota: Perfluorobutane Sulfonamide in Several Fish Species, Environ. Sci. Techno. 50 (2016) 669.
[5] M.S. Tsai, M.H. Chen, C.C. Lin, S. Ng, C.J. Hsieh, C.Y. Liu, W.S. Hsieh, P.C. Chen, Children's environmental health based on birth cohort studies of Asia, Sci. Total Environ. 609 (2017) 396.
[6] S.J. Ye, G.M. Zeng, H.P. Wu, C. Zhang, J. Liang, J. Dai, Z.F. Liu, W.P. Xiong, J. Wan, P.A. Xu, M. Cheng, Co-occurrence and interactions of pollutants, and their impacts on soil remediation-A review, Crit. Rev. Environ. Sci. Technol. 47 (2017) 1528–1553.
[7] P. Meng, X. Fang, A. Maimaiti, G. Yu, S. Deng, Efficient removal of perfluorinated compounds from water using a regenerable magnetic activated carbon, Chemosphere 224 (2019) 187–194.
[8] B.O. Fagbayigbo, B.O. Opeolu, O.S. Fatoki, T.A. Akenga, O.S. Olatunji, Removal of PFOA and PFOS from aqueous solutions using activated carbon produced from Vitis vinifera leaf litter, Environ. Sci. Pollut. Res. 24 (2017) 1–14.
[9] N.A. Fernandez, L. Rodriguez-Freire, M. Keswani, R. Sierra-Alvarez, Effect of chemical structure on the sonochemical degradation of perfluoroalkyl and polyfluoroalkyl substances (PFASs), Environ. Sci.-Wat. Res. Technol. 2 (2016).
[10] Y.C. Lee, S.L. Lo, J. Kuo, Y.L. Lin, Persulfate oxidation of perfluorooctanoic acid under the temperatures of 20–40 °C, Chem. Eng. J. s 198–199 (2012) 27–32.
[11] D.H. Huang, L.F. Yin, J.F. Niu, Photoinduced Hydrodefluorination Mechanisms of Perfluorooctanoic Acid by the SiC/Graphene Catalyst, Environ. Sci. Techno. 50 (2016) 5857–5863.
[12] Y. Yang, C. Zhang, C. Lai, G.M. Zeng, D.L. Huang, M. Cheng, J.J. Wang, F. Chen, C.Y. Zhou, W.P. Xiong, BiOX (X = Cl, Br, I) photocatalytic nanomaterials: applications for fuels and environmental management, Adv. Colloid Interface Sci. 254 (2018) 76–93.
[13] A. Alsbaiee, B.J. Smith, L.L. Xiao, Y.H. Ling, D.E. Helbling, W.R. Dichtel, Rapid removal of organic micropollutants from water by a porous beta-cyclodextrin polymer, Nature 529 (2016) 190–U146.
[14] J.L. Gong, B. Wang, G.M. Zeng, C.P. Yang, C.G. Niu, Q.Y. Niu, W.J. Zhou, Y. Liang, Removal of cationic dyes from aqueous solution using magnetic multi-wall carbon nanotube nanocomposite as adsorbent, J. Hazard. Mater. 164 (2009) 1517–1522.
[15] D.N. Jiang, M. Chen, H. Wang, G.M. Zeng, D.L. Huang, M. Cheng, Y. Liu, W.J. Xue, Z.W. Wang, The application of different typological and structural MOFs-based materials for the dyes adsorption, Coord. Chem. Rev. 380 (2019) 471–483.
[16] A. Khataee, M. Sheydaei, A. Hassani, M. Taseidifar, S. Karaca, Sonocatalytic removal of an organic dye using TiO2/Montmorillonite nanocomposite, Ultrason. Sonochem. 22 (2015) 404–411.
[17] Z.Z. Huang, K. He, Z.X. Song, G.M. Zeng, A.W. Chen, L. Yuan, H. Li, L. Hu, Z. Guo, G.Q. Chen, Antioxidative response of Phanerochaete chrysosporium against silver nanoparticle-induced toxicity and its potential mechanism, Chemosphere 211 (2018) 573–583.
[18] D.B. Miklos, C. Remy, M. Jekel, K.G. Linden, J.E. Drewes, U. Hubner, Evaluation of advanced oxidation processes for water and wastewater treatment - a critical review, Water Res. 139 (2018) 118–131.
[19] K. He, G.Q. Chen, G.M. Zeng, A.W. Chen, Z.Z. Huang, J.B. Shi, T.T. Huang, M. Peng, L. Hu, Three-dimensional graphene supported catalysts for organic dyes degradation, Appl. Catal. B-Environ. 228 (2018) 19–28.
[20] I.A. Ike, K.G. Linden, J.D. Orbell, M. Duke, Critical review of the science and sustainability of persulphate advanced oxidation processes, Chem. Eng. J. 338 (2018) 651–669.
[21] Y. X. Bao, S. S. Deng, X. S. Jiang, Y. X. Qu, Y. He, L. Q. Liu, Q. W. Chai, M. Mumtaz, J. Huang, G. Cagnetta, G. Yu, Degradation of PFOA Substitute: GenX (HFPO-DA Ammonium Salt): Oxidation with UV/Persulfate or Reduction with UV/Sulfite?, Environ. Sci. Techno. 52 (201820) 11728-11734.
[22] S. Norzaee, M. Taghavi, B. Djahed, F.M. Kord, Degradation of Penicillin G by heat activated persulfate in aqueous solution, J. Environ. Manage. 215 (2018) 316–323.
[23] J.E. Silveira, W.S. Paz, J.A. Zazo, J.A. Casas, UV-LED/ilmenite/persulfate for azo dye mineralization: the role of sulfate in the catalyst deactivation, Appl. Catal. B-Environ. 219 (2017) 314–321.
[24] Y. Xu, H. Lin, Y. Li, H. Zhang, The mechanism and efficiency of MnO2 activated persulfate process coupled with electrolysis, Sci. Total Environ. 609 (2017) 644–654.
[25] R.Y. Xiao, Z.H. Luo, Z.S. Wei, S. Luo, R. Spinney, W.C. Yang, D.D. Dionysiou, Activation of peroxymonosulfate/persulfate by nanomaterials for sulfate radical-based advanced oxidation technologies, Curr. Opin. Chem. Eng. 19 (2018) 51–58.
[26] K. He, Z.T. Zeng, A.W. Chen, G.M. Zeng, R. Xiao, P. Xu, Z.Z. Huang, J.B. Shi, L. Hu, G.Q. Chen, Advancement of Ag-Graphene Based Nanocomposites: An Overview of Synthesis and Its Applications, Small 14 (2018).
[27] C.Y. Zhou, C. Lai, C. Zhang, G.M. Zeng, D.L. Huang, M. Cheng, L. Hu, W.P. Xiong, M. Chen, J.J. Wang, Y. Yang, L.B. Jiang, Semiconductor/boron nitride composites:

synthesis, properties, and photocatalysis applications, Appl. Catal. B-Environ. 238 (2018) 6–18.
[28] M.J. Zhang, Y. Zhang, L. Tang, G.M. Zeng, J.J. Wang, Y. Zhu, C.Y. Feng, Y.C. Deng, W.Z. He, Ultrathin Bi2WO6 nanosheets loaded g-C3N4 quantum dots: a direct Z-scheme photocatalyst with enhanced photocatalytic activity towards degradation of organic pollutants under wide spectrum light irradiation, J. Colloid Interface Sci. 539 (2019) 654–664.
[29] Y.R. Wang, Y. Zhu, Y. Hu, G.M. Zeng, Y. Zhang, C. Zhang, C.L. Feng, How to Construct DNA Hydrogels for Environmental Applications: Advanced Water Treatment and Environmental Analysis, Small 14 (2018).
[30] X. Tang, G.M. Zeng, C.Z. Fan, M. Zhou, L. Tang, J.J. Zhu, J. Wan, D.L. Huang, M. Chen, P. Xu, C. Zhang, Y. Lu, W.P. Xiong, Chromosomal expression of CadR on Pseudomonas aeruginosa for the removal of Cd(II) from aqueous solutions, Sci. Total Environ. 636 (2018) 1355–1361.
[31] H. Wang, Z.T. Zeng, P. Xu, L.S. Li, G.M. Zeng, R. Xiao, Z.Y. Tang, D.L. Huang, L. Tang, C. Lai, D.N. Jiang, Y. Liu, H. Yi, L. Qin, S.J. Ye, X.Y. Ren, W.W. Tang, Recent progress in covalent organic framework thin films: fabrications, applications and perspectives, Chem. Soc. Rev. 48 (2019) 488–516.
[32] S.J. Ye, G.M. Zeng, H.P. Wu, C. Zhang, J. Dai, J. Liang, J.F. Yu, X.Y. Ren, H. Yi, M. Cheng, C. Zhang, Biological technologies for the remediation of co-contaminated soil, Crit. Rev. Biotechnol. 37 (2017) 1062–1076.
[33] L. Betancor, H.R. Luckarift, Bioinspired enzyme encapsulation for biocatalysis, Trends Biotechnol. 26 (2008) 566–572.
[34] H.J. Cheng, L. Zhang, J. He, W.J. Guo, Z.Y. Zhou, X.J. Zhang, S.M. Nie, H. Wei, Integrated Nanozymes with Nanoscale Proximity for in Vivo Neurochemical Monitoring in Living Brains, Anal. Chem. 88 (2016) 5489–5497.
[35] J.P. Collman, X. Zhang, V.J. Lee, E.S. Uffelman, J.I. Brauman, Regioselective and enantioselective epoxidation catalyzed by metalloporphyrins, Science 261 (1993) 1404–1411.
[36] P.A. Xu, G.M. Zeng, D.L. Huang, C.L. Feng, S. Hu, M.H. Zhao, C. Lai, Z. Wei, C. Huang, G.X. Xie, Z.F. Liu, Use of iron oxide nanomaterials in wastewater treatment: a review, Sci. Total Environ. 424 (2012) 1–10.
[37] W.P. Xiong, Z.T. Zeng, X. Li, G.M. Zeng, R. Xiao, Z.H. Yang, Y.Y. Zhou, C. Zhang, M. Cheng, L. Hu, C.Y. Zhou, L. Qin, R. Xu, Y.R. Zhang, Multi-walled carbon nanotube/amino-functionalized MIL-53(Fe) composites: remarkable adsorptive removal of antibiotics from aqueous solutions, Chemosphere 210 (2018) 1061–1069.
[38] Y.D. Chen, S.H. Ho, D. Wang, Z.S. Wei, J.S. Chang, N.Q. Ren, Lead removal by a magnetic biochar derived from persulfate-ZVI treated sludge together with one-pot pyrolysis, Bioresour. Technol. 247 (2017) 463–470.
[39] D. Ouyang, J. Yan, L. Qian, Y. Chen, L. Han, A. Su, W. Zhang, N. Hao, M. Chen, Degradation of 1,4-Dioxane by Biochar Supported Nano Magnetite Particles Activating Persulfate, Chemosphere 184 (2017) 609–617.
[40] Y. Zang, J. Lei, L. Zhang, H. Ju, In situ generation of electron acceptor for photoelectrochemical biosensing via hemin-mediated catalytic reaction, Anal. Chem. 86 (2014) 12362–12368.
[41] S. Deng, J. Lei, Y. Huang, Y. Cheng, H. Ju, Electrochemiluminescent quenching of quantum dots for ultrasensitive immunoassay through oxygen reduction catalyzed by nitrogen-doped graphene-supported hemin, Anal. Chem. 85 (2013) 5390.
[42] G. Huang, Y. Liu, J.L. Cai, X.F. Chen, S.K. Zhao, Y.A. Guo, S.J. Wei, X. Li, Heterogeneous biomimetic catalysis using iron porphyrin for cyclohexane oxidation promoted by chitosan, Appl. Surf. Sci. 402 (2017) 436–443.
[43] B. Song, M. Chen, S.J. Ye, P. Xu, G.M. Zeng, J.L. Gong, J. Li, P. Zhang, W.C. Cao, Effects of multi-walled carbon nanotubes on metabolic function of the microbial community in riverine sediment contaminated with phenanthrene, Carbon 144 (2019) 1–7.
[44] M. Darder, P. Aranda, E. Ruiz-Hitzky, Bionanocomposites: a new concept of ecological, bioinspired, and functional hybrid materials, Adv. Mater. 19 (2007) 1309–1319.
[45] C. Zhang, W.J. Wang, A.B. Duan, G.M. Zeng, D.L. Huang, C. Lai, X.F. Tan, M. Cheng, R.Z. Wang, C.Y. Zhou, W.P. Xiong, Y. Yang, Adsorption behavior of engineered carbons and carbon nanomaterials for metal endocrine disruptors: experiments and theoretical calculation, Chemosphere 222 (2019) 184–194.
[46] E.S. Penido, G.C. Martins, T.B.M. Mendes, L.C.A. Melo, I.D. Guimaraes, L.R.G. Guilherme, Combining biochar and sewage sludge for immobilization of heavy metals in mining soils, Ecotox. Environ. Safe. 172 (2019) 326–333.
[47] A. Ashiq, N.M. Adassooriya, B. Sarkar, A.U. Rajapaksha, Y.S. Ok, M. Vithanage, Municipal solid waste biochar-bentonite composite for the removal of antibiotic ciprofloxacin from aqueous media, J. Environ. Manage. 236 (2019) 428–435.
[48] M.J. Ahmed, P.U. Okoye, E.H. Hummadi, B.H. Hameed, High-performance porous biochar from the pyrolysis of natural and renewable seaweed (Gelidiella acerosa) and its application for the adsorption of methylene blue, Bioresour. Technol. 278 (2019) 159–164.
[49] L.H. Zhang, J.C. Zhang, G.M. Zeng, H.R. Dong, Y.N. Chen, C. Huang, Y. Zhu, R. Xu, Y.J. Cheng, K.J. Hou, W.C. Cao, W. Fang, Multivariate relationships between microbial communities and environmental variables during co-composting of sewage sludge and agricultural waste in the presence of PVP-AgNPs, Bioresour. Technol. 261 (2018) 10–18.
[50] S.J. Ye, M. Yan, X.F. Tan, J. Liang, G.M. Zeng, H.P. Wu, B. Song, C.Y. Zhou, Y. Yang, H. Wang, Facile assembled biochar-based nanocomposite with improved graphitization for efficient photocatalytic activity driven by visible light, Appl. Catal. B-Environ. 250 (2019) 78–88.
[51] G. Fang, C. Zhu, D.D. Dionysiou, J. Gao, D. Zhou, Mechanism of hydroxyl radical generation from biochar suspensions: implications to diethyl phthalate degradation, Bioresour. Technol. 176 (2015) 210.
[52] W.J. Wang, P. Xu, M. Chen, G.M. Zeng, C. Zhang, C.Y. Zhou, Y. Yang, D.L. Huang, C. Lai, M. Cheng, L. Hu, W.P. Xiong, H. Guo, M. Zhou, Alkali Metal-Assisted Synthesis of Graphite Carbon Nitride with Tunable Band-Gap for Enhanced Visible-Light-Driven Photocatalytic Performance, ACS Sustain. Chen. Eng. 6 (2018) 15503–15516.
[53] L. Khachatryan, E. Vejerano, S. Lomnicki, B. Dellinger, Environmentally persistent free radicals (EPFRs). 1. Generation of reactive oxygen species in aqueous solutions, Environ. Sci. Techno. 45 (2013) 8559–8566.
[54] J.N. Yang, X.R. Liu, D.B. Wang, Q.X. Xu, Q. Yang, G.M. Zeng, X.M. Li, Y.W. Liu, J.L. Gong, J. Ye, H.L. Li, Mechanisms of peroxymonosulfate pretreatment enhancing production of short-chain fatty acids from waste activated sludge, Water Res. 148 (2018) 239–249.
[55] I. Hussain, M. Li, Y. Zhang, Y. Li, S. Huang, X. Du, G. Liu, W. Hayat, N. Anwar, Insights into the mechanism of persulfate activation with nZVI/BC nanocomposite for the degradation of nonylphenol, Chem. Eng. J. (2017).
[56] H. Yi, M. Yan, D.L. Huang, G.M. Zeng, C. Lai, M.F. Li, X.Q. Huo, L. Qin, S.Y. Liu, X.G. Liu, B.S. Li, H. Wang, M.C. Shen, Y.K. Fu, X.Y. Guo, Synergistic effect of artificial enzyme and 2D nano-structured Bi2WO6 for eco-friendly and efficient biomimetic photocatalysis, Appl. Catal. B-Environ. 250 (2019) 52–62.
[57] X.M. Xu, S.Y. Zong, W.M. Chen, D. Liu, Comparative study of Bisphenol A degradation via heterogeneously catalyzed H2O2 and persulfate: reactivity, products, stability and mechanism, Chem. Eng. J. 369 (2019) 470–479.
[58] L.R. Bennedsen, J. Muff, E.G. Sogaard, Influence of chloride and carbonates on the reactivity of activated persulfate, Chemosphere 86 (2012) 1092–1097.
[59] X.F. Zhao, C.G. Niu, L. Zhang, H. Guo, X.J. Wen, C. Liang, G.M. Zeng, Co-Mn layered double hydroxide as an effective heterogeneous catalyst for degradation of organic dyes by activation of peroxymonosulfate, Chemosphere 204 (2018) 11–21.